Letters

Globally Stable Speed-Adaptive Observer With Auxiliary States for Sensorless Induction Motor Drives

Jiahao Chen, *Student Member, IEEE*, and Jin Huang

***Abstract*—This letter responds to one question raised in the literature: whether or not global stability of speed estimation is possible to attain for sensorless induction motor drives. The answer is affirmative, excluding the zero-frequency operation that corresponds to the unobservable set of motor speed.**

***Index Terms*—Global stability, instability, regeneration mode, sensorless drive, slow-speed-reversal test.**

I. Introduction

STABILIZATION in regeneration mode is one of the remaining topics in the very mature field of sensorless induction motor (IM) drives, which has drawn a lot of attention. During regenerating operation, various instability phenomena will probably occur, of which several types are summarized in the survey paper [1].

Global stability of speed estimation has been pursued in the literature. Particularly, it has been shown that the attempts to establish a Lyapunov function for the structure of full-order observer [2] or for the structure of model reference adaptive system (MRAS) [3] will not succeed. Besides, there is also endeavor to show that the speed-adaptive full-order observer can be made globally stable by a proper selection of feedback gains based on the positive real property [4], [5], but the proposed selection of feedback gains is unrealistic owing to the dependence of the actual speed [6]. Similarly, a recent work of speed-adaptive sliding mode observer proposes a time-varying feedback gain selection that relies on the actual motor speed [7].

As a result, remedies are offered to obtain local stability, such as the *complete stability conditions* [8], and the linearized model based analysis [6], [9]–[11]. Particularly, the *relative stability* of speed estimation is further concerned in [11]. In addition, recent works on developing new MRAS schemes are

Manuscript received January 31, 2018; revised April 26, 2018; accepted May 8, 2018. Date of publication May 14, 2018; date of current version November 19, 2018. This work was supported in part by the National Key Basic Research Program of China (973 Project) under Grant 2013CB035604 and in part by the major program of the National Natural Science Foundation of China under Grant 51690182. *(Corresponding author: Jiahao Chen.)*

The authors are with the College of Electrical Engineering, Zhejiang University, Hangzhou 310027, China (e-mail:

whose dimensions are, respectively, Weber and Volt. The dynamics of ψ_σ and χ are derived as

$$\begin{aligned} p\psi_\sigma &= \chi - (\alpha L_s + r_s)\, i_s + \omega J \psi_\sigma + u_s \\ p\chi &= \alpha u_s - \omega J u_s - \alpha r_s i_s + \omega r_s J i_s \end{aligned} \tag{3}$$

where $L_s = L_\mu + L_\sigma$ is the stator inductance. Note that χ is now the unmeasured state, and apparently, the regressive vector for ω relies on the knowledge of voltages, currents, and stator-side parameters (i.e., r_s and L_σ), which are all presumed to be available.

B. Speed-Adaptive Observer Design

We use a $\hat{}$ to designate estimated quantity, and define the output error $\varepsilon = \psi_\sigma - \hat{\psi}_\sigma$. One possible adaptive observer for (3) can be established as

$$\begin{cases} p\hat{\psi}_\sigma = \hat{\chi} + (u_s - r_s i_s - \alpha L_s i_s) + J\psi_\sigma \hat{\omega} + \lambda_1 \varepsilon + \upsilon^1 p\hat{\omega} \\ p\hat{\chi} = \alpha\,(u_s - r_s i_s) - J\,(u_s - r_s i_s)\,\hat{\omega} + \lambda_2 \varepsilon + \upsilon^2 p\hat{\omega} \\ p\upsilon^1 = -\lambda_1 \upsilon^1 + \upsilon^2 + J\psi_\sigma \\ p\upsilon^2 = -\lambda_2 \upsilon^1 - J(u_s - r_s i_s) \\ p\hat{\omega} = \gamma_\omega \varepsilon^T \upsilon^1 \end{cases} \tag{4}$$

where $\upsilon^1, \upsilon^2 \in \mathbb{R}^2$ designate the filtered regressive vectors, γ_ω is the positive adaptation gain, and λ_1, λ_2 are the positive feedback gains. It is shown in [17, Th. 1] that the stability of the adaptive observer (4) holds with global and exponential convergence, if the criterion for persistency of excitation (PE)

$$a \le \int_t^{t+T} \upsilon^{1T} \upsilon^1 dt \le b \tag{5}$$

suffices with positive constants T, a, b for all t.

At steady state, one can calculate υ^1 in the d-q frame rotating at the synchronous speed ω_ψ by

$$\begin{cases} \upsilon_d^1 = \dfrac{C_0}{C_2^2 + C_1^2}\,(C_1 \mathrm{temp1} - C_2 \mathrm{temp2}) + \lambda_2^{-1}\,(u_{qs} - r_s i_{qs}) \\ \upsilon_q^1 = -\dfrac{C_0}{C_2^2 + C_1^2}\,(C_1 \mathrm{temp2} + C_2 \mathrm{temp1}) - \lambda_2^{-1}\,(u_{ds} - r_s i_{ds}) \end{cases} \tag{6}$$

with

$$\mathrm{temp1} = \lambda_1 \lambda_2^{-1}\,(u_{ds} - r_s i_{ds}) - \lambda_2^{-1} \omega_\psi\,(u_{qs} - r_s i_{qs}) + \psi_{d\sigma}$$

$$\mathrm{temp2} = -\lambda_1 \lambda_2^{-1}\,(u_{qs} - r_s i_{qs}) - \lambda_2^{-1} \omega_\psi\,(u_{ds} - r_s i_{ds}) - \psi_{q\sigma}$$

and $C_0 = \lambda_2^{-1}\omega_\psi$, $C_1 = 1 - \lambda_2^{-1}\omega_\psi \omega_\psi$, and $C_2 = \lambda_1 \lambda_2^{-1} \omega_\psi$, which implies that the synchronous speed ω_ψ should be different from null to achieve PE. In other words, the sensorless IM drive should avoid zero-frequency operation.

In addition, the computed rotor flux $\hat{\psi}_\mu$ can as well be recovered by

$$\hat{\psi}_\mu = \left(\alpha^2 + \hat{\omega}^2\right)^{-1} (\alpha I + \hat{\omega} J)\, \hat{\chi} - \hat{\psi}_\sigma \tag{7}$$

IV. Experimental Results

With the above-mentioned speed-adaptive observer (4), the sensorless control of IM can be implemented (see, e.g., [18]), for which the expected performance should include stable operation in both motoring and regeneration mode.

A. Test Bench Setup

The IM, whose nameplate data are 4 kW, 50 Hz, 1440 r/min, 380 V, and 8.8 A, is driven by a voltage-source inverter. The load torque is provided by a separately excited dc generator, and it is computed by $T_L = K_{dc} i_{\mathrm{Load}}$ with K_{dc} the dc torque factor and i_{Load} the measured armature current. Particularly, the regenerative load torque is produced by connecting the armature of the dc generator to the dc bus. The numerical values of the tested motor and the design coefficients are listed in Appendix.

B. Sensorless Slow-Speed-Reversal Test

The sensorless slow-speed-reversal test is deemed to be an effective way to test whether a sensorless scheme is still stable in the regeneration mode [1]. The results of the experiment using the proposed observer during the sensorless slow-speed-reversal test are shown in Fig. 1, in which the waveforms of ω, $\hat{\omega}$, i_{Ts} (torque producing current), T_L, ω_ψ (synchronous speed), i_{Ms} (magnetizing current), and the phase current are sketched, and the torque–speed characteristics are also plotted using the same data of ω, $\hat{\omega}$, and T_L. The slow speed reversal takes 40 s from 100 to -100 r/min, which corresponds to a changing rate of the ramp speed command of -5 r/min/s. It is observed that the sensorless drive operates stably in both motoring and regenerating conditions, but when ω_ψ becomes near the vicinity of null, the estimated speed $\hat{\omega}$ deviates from the actual speed ω owing to the lack of PE, as highlighted by the shaded window in Fig. 1(a). The successful zero frequency crossing is due to the observer's relative stability near the zero frequency, as well as the variation in speed command that can be considered as a nonsteady state excitation. In other words, it works because the slow speed reversal is not slow enough.

As a matter of fact, the sensorless drive would become unstable if the changing rate of the ramp speed command is slowed to -2 r/min/s, as shown in Fig. 2. This should be easily understood that according to (5) and (6), the adaptive observer will possibly lose its stability if the motor is under a steady state excitation of zero frequency. Thus, in the limit when the slow speed reversal is so slow that the time spent near the zero frequency is long enough to consider the motor excitation as a steady state zero frequency excitation, the unstable phenomenon may occur, in which the speed estimated error ($\tilde{\omega} \triangleq \omega - \hat{\omega}$) diverges and the actual slip frequency becomes so large that the torque produced is very limited.

One may conclude that the proposed sensorless drive can operate at both motoring and regenerating conditions. Though dwelling at zero stator frequency is not stable owing to the loss of PE, zero frequency crossing is possible provided that the changing rate of the ramp speed command is not too low.

C. Avoidance of Zero Frequency Operation

As shown by the experimental results from Fig. 2, the unstable operation is predicted by the loss of PE, i.e., zero frequency

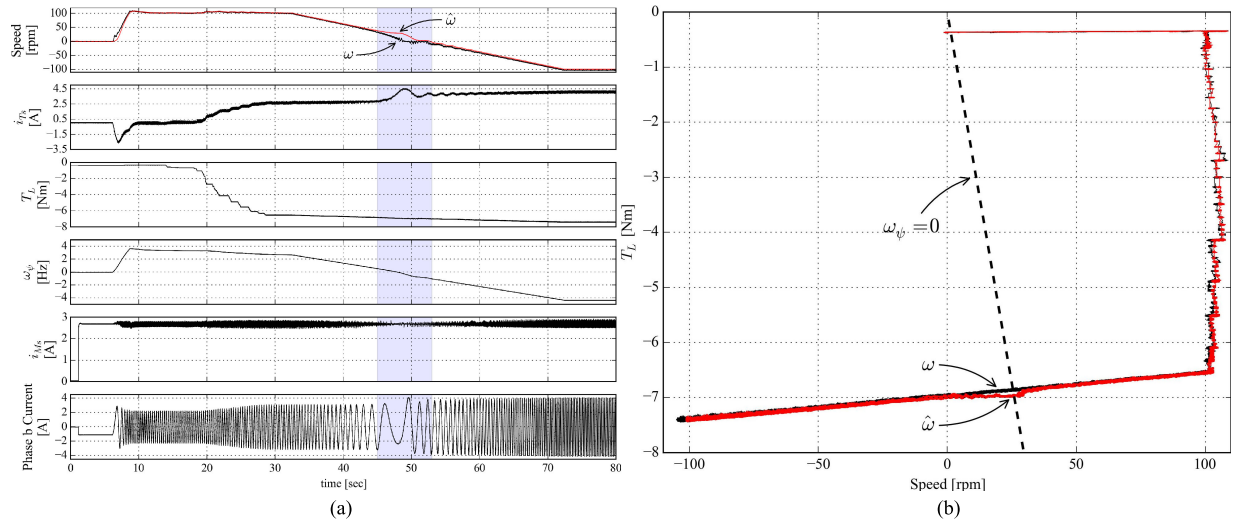

Fig. 1. Experimental sensorless slow-speed-reversal test with a deceleration rate of 5 r/min/s. (a) Waveforms during the test. (b) Torque–speed characteristics.

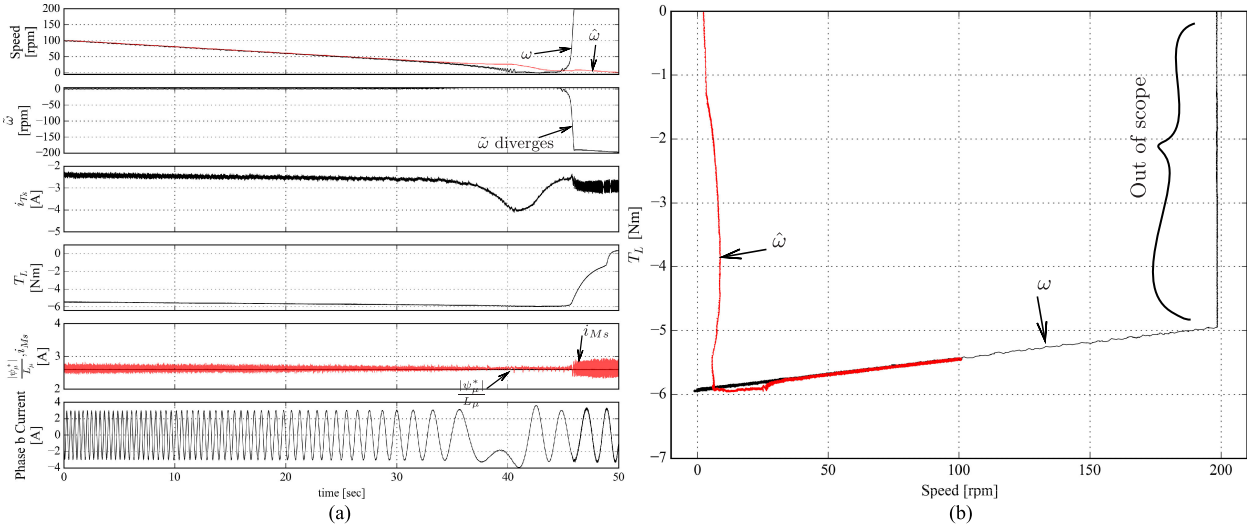

Fig. 2. Experimental sensorless slow-speed-reversal test with a deceleration rate of 2 r/min/s. (a) Waveforms during the test. (b) Torque–speed characteristics.

excitation. Hence, different strategies have been proposed for avoidance of zero frequency operation [19], [20]. The idea is to manipulate the slip frequency to avoid zero synchronous frequency, by selecting flux modulus command according to proper criteria. However, the performance of those strategies depends on motor parameters. For motor with smaller rotor resistance, those methods could become less effective.

Another solution to attain the ability of zero frequency operation resorts to high-frequency signal injection, which is criticized by its cause to toque ripples [21]. However, the method based on the injection of a high-frequency fluctuating signal in the synchronously rotating reference frame [22] claims no torque ripple exists after the field is orientated. Anyway, signal injection incurs additional copper, eddy-current, and hysteresis loss.

As an example, to make sense of the idea of slip frequency manipulation, we redo the 2-r/min/s-deceleration slow speed reversal with avoidance of zero frequency operation and the results are shown in Fig. 3. Let $\omega_{sl} \propto \frac{i_{Ts}}{i_{Ms}}$ denote the slip angular

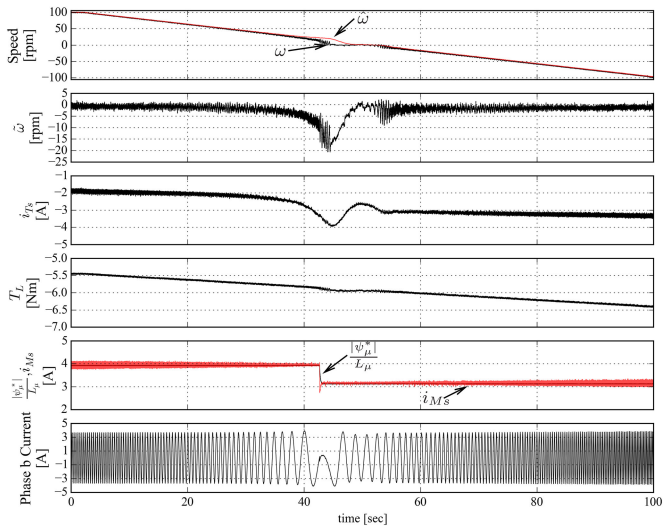

Fig. 3. Experimental sensorless slow-speed-reversal test with a deceleration rate of 2 r/min/s and avoidance of zero frequency operation.

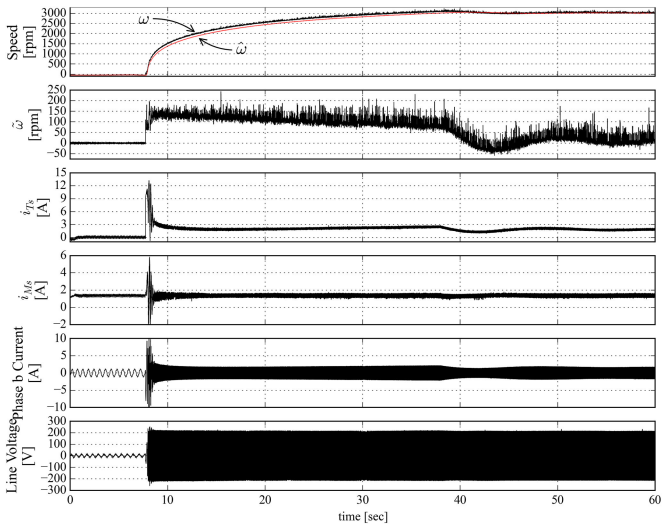

Fig. 4. Experimental sensorless high-speed step response (-50 r/min to 3000 r/min).

speed. At $t \approx 42.5$ s, as the speed decreases such that $\hat{\omega} + \omega_{sl}$ approaches 0 from the above, a negative step change in ω_{sl} is imposed by altering the magnetizing current i_{Ms}, which helps the sensorless drive to skip the zero frequency excitation. As a result, zero frequency operation never practically happens, so the slow zero frequency crossing will succeed.

D. High-Speed Operation

In Fig. 4, the experimental results of the sensorless drive operating at flux weakening region are presented. The commanded speed is 3000 r/min, which is nearly two times the rated speed of the tested IM. Current oscillation is observed when the 3000 r/min command is applied at $t \approx 8$ s because of coupling between M-axis and T-axis voltage equations.[1] Speed estimated error $\tilde{\omega} \triangleq \omega - \hat{\omega}$ exists during the acceleration, while after reaching steady state, $\tilde{\omega}$ converges toward 0 r/min. As a result, one concludes that the proposed adaptive observer has the potential to reach a wide speed operating range.

E. Influence of Parameter Uncertainty

1) Leakage Inductance Uncertainty: As stated in [1], the (total) leakage inductance is not critical, for an erroneous value does not affect the produced torque. On the other hand, since we use $\psi_\sigma = L_\sigma i_s$ as system output, it seems that the leakage inductance error ($\tilde{L}_\sigma \triangleq L_\sigma - \hat{L}_\sigma$) has a large effect on the output error $\varepsilon = \psi_\sigma - \hat{\psi}_\sigma$. However, from the experimental results given in Fig. 5, it is observed that $\tilde{L}_\sigma$ has little influence on speed estimation performance. Specifically, during low-speed operation, as the leakage inductance value $\hat{L}_\sigma$ decreases to $5\%L_\sigma$, a speed estimated error of $\tilde{\omega} = -1.5$ r/min is observed; on the other hand, an overestimated value of $\hat{L}_\sigma = 300\%L_\sigma$ results in a speed estimated error of $\tilde{\omega} = 3$ r/min. As for high-speed operation, as the leakage inductance value ranges from $5\%L_\sigma$ to $300\%L_\sigma$, the average speed estimated error is below 50 r/min. For both low-speed and high-speed situations, an overestimated leakage inductance has a severer impact on speed estimation than an underestimated one.

This result can be explained as follows. Take a look at (1a), one realizes that for an open-loop current observer, the parameter L_σ is in charge of how fast the current estimation varies, and then in this case, $\tilde{L}_\sigma$ will cause current estimated error as well as biased speed estimation. On the other hand, the observer (4) is *per se* also a current observer but it is a closed-loop one, which means that the changing rate of the current estimation is also determined by the (output error) feedback terms with $\lambda_1 > 0$. Even if there is uncertainty in $\hat{L}_\sigma$, the current estimated error $i_s - \hat{i}_s$ will become very limited by using a sufficiently large λ_1. Moreover, since L_σ is unknown, we can only compute the output error by $\varepsilon = \hat{L}_\sigma i_s - \hat{L}_\sigma \hat{i}_s = \hat{L}_\sigma (i_s - \hat{i}_s)$, which is merely current estimated error scaled by $\hat{L}_\sigma$. So, the influence of $\tilde{L}_\sigma$ is expected to be small.

2) Stator Resistance Uncertainty: Stator resistance is a critical parameter for low-speed operation of a sensorless drive [10]. Without exception, the proposed adaptive observer may lose its stability if exposed to a large error in stator resistance. To see this, sensorless control experiments under stator resistance uncertainty are carried out, and the results of overestimated case and underestimated case are shown, respectively, in Fig. 6(a) and (d). For both cases, when the stator resistance error is within $[-50\%r_s, 50\%r_s]$, the speed estimation only becomes biased, whereas further growing of stator resistance error may make the speed estimation diverge. Practical remedies to stator resistance uncertainty have been reviewed in [1] and [23].

V. Discussion

A. Rotor Resistance Estimation

There is argument that rotor resistance uncertainty will not cause stationary torque errors in a direct field oriented controlled sensorless drive [4], [24], but it will degrade the speed control accuracy if the sensorless drive is loaded.

Fortunately, one can further show that with the choice of the auxiliary states (2), the joint estimation of ω and r_{req} is as well possible by imposing a second-order PE condition.

Denoting $x = [\psi_\sigma^T, \chi^T]^T$, rewrite the dynamics (3) into the matrix form

$$\begin{aligned} px &= Ax + \phi_0 + \Phi\theta \\ \psi_\sigma &= Cx \end{aligned} \tag{8}$$

where $C = \begin{bmatrix} I & 0 \end{bmatrix}$, $\phi_0 = \begin{bmatrix} (u_s - r_s i_s)^T, 0 \end{bmatrix}^T$, $\theta = [\alpha, \omega]^T$ is the parameter vector, while the homogeneous matrix A and the linear-in-parameters regressive matrix Φ are respectively

$$A = \begin{bmatrix} 0 & I \\ 0 & 0 \end{bmatrix}, \ \Phi = \begin{bmatrix} -L_s i_s & L_\sigma J i_s \\ u_s - r_s i_s & -J(u_s - r_s i_s) \end{bmatrix}.$$

[1]We denote field-oriented frame as M–T frame, where M-axis is aligned with the rotor flux vector and T-axis is 90° leading to the M-axis.

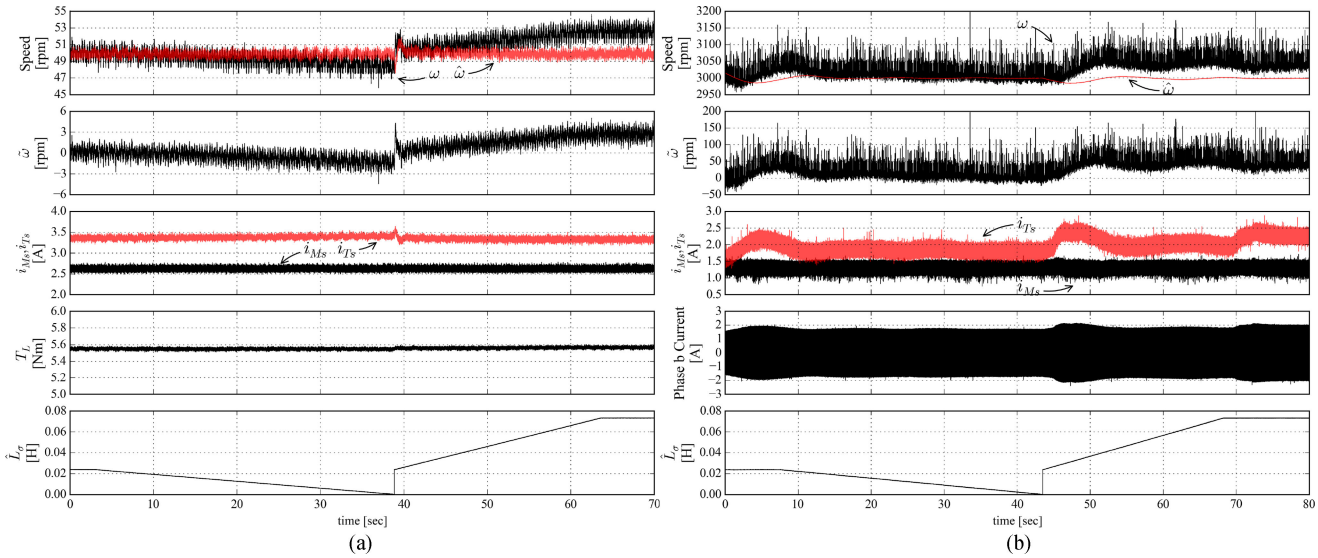

Fig. 5. Experimental sensorless control under total leakage inductance uncertainty. (a) Low-speed operation. (b) High-speed operation.

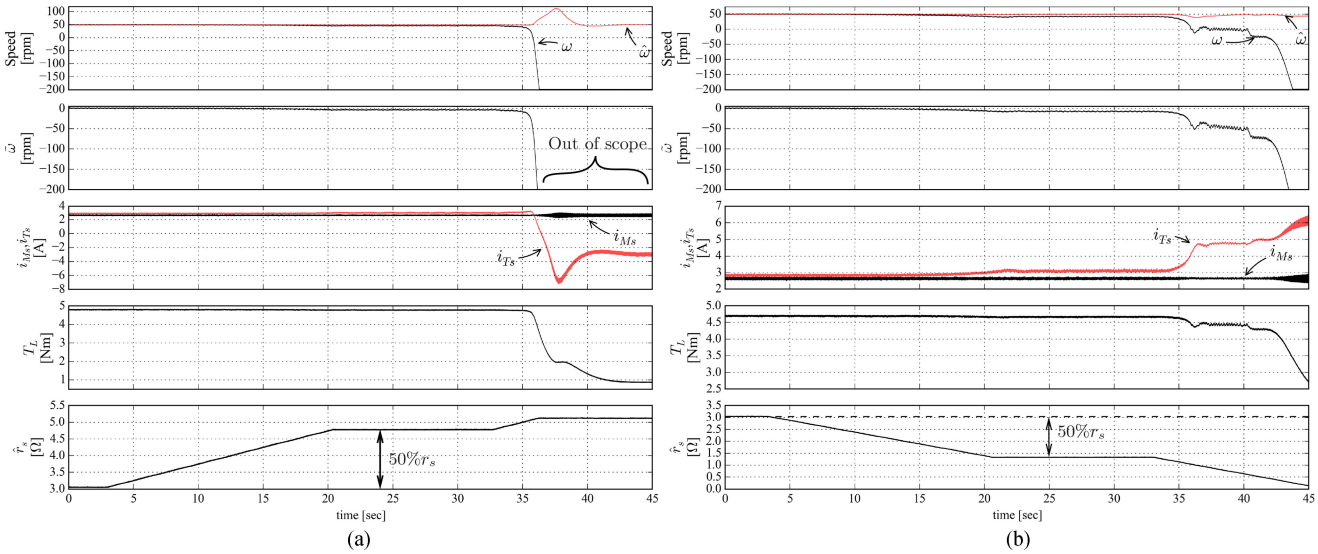

Fig. 6. Experimental sensorless control under stator resistance uncertainty. (a) Overestimated case. (b) Underestimated case.

The observer that is adaptive to ω and α can be written concisely as follows [17]:

$$\begin{cases} p\hat{x} = A\hat{x} + \phi_0 + \Phi\hat{\theta} + KC\left(x - \hat{x}\right) + \Upsilon\dot{\hat{\theta}} \\ p\hat{\theta} = \Gamma\Upsilon^T C^T C\left(x - \hat{x}\right) \\ p\Upsilon = \left(A - KC\right)\Upsilon + \Phi, \quad \Upsilon\left(0\right) = 0 \end{cases} \tag{9}$$

where $\Gamma \in \mathbb{R}^{2\times 2}$ is the diagonal adaptation gain matrix, $\Upsilon \in \mathbb{R}^{4\times 2}$ is the filtered regressive matrix, and $K = [k_1 I, k_2 I]^T$ is the feedback gain matrix with $k_1, k_2 \in \mathbb{R}_{>0}$. The corresponding PE condition is

$$aI \leq \int_t^{t+T} \Upsilon^T\left(t\right) C^T C \Upsilon\left(t\right) dt \leq bI.$$

with some positive constants T, a, b for all t.

To verify the effectiveness of the design, experiment for joint estimation of r_{req} and ω is conducted, and the results are shown in Fig. 7, where to improve the parameter identification capability, a low-frequency (1 Hz, 0.05 A) sinusoidal component is added to the magnetizing current i_{Ms}. To test the system robustness with respect to rotor resistance uncertainty, we deliberately set $\hat{r}_{\text{req}}$ to $140\%r_{\text{req}}$ at $t = 6.5$ s, which causes a speed estimated error maximum of 11 r/min, and in the meanwhile we turn on the adaptation of r_{req}. As a result, rotor resistance is identified and the speed control accuracy is improved at loaded conditions. However, speed ripples result because of the low-frequency component in i_{Ms}.

Remark: The simultaneous estimation of ω, r_{req}, and r_s is, however, nothing intuitive owing to the nonlinear parametrization of (3), for which further research needs to be carried out.

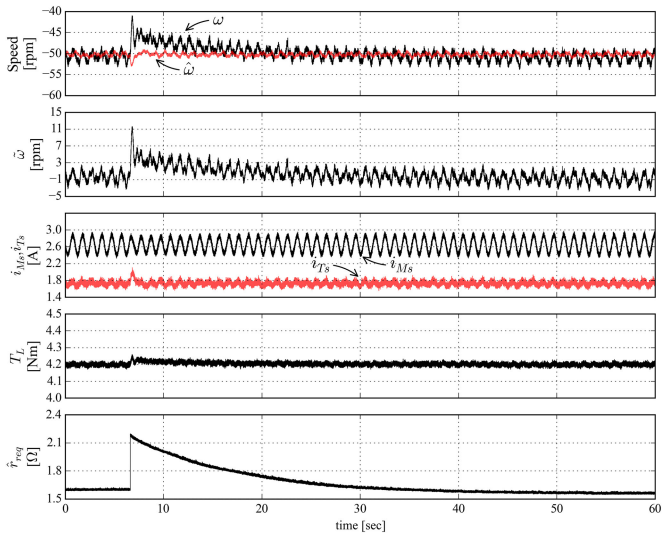

Fig. 7. Experiment for joint estimation of r_{req} and ω in regenerating operation with $\Gamma = \text{diag}\,(1\text{e}5, \gamma_\omega)$, $k_1 = \lambda_1$, and $k_2 = \lambda_2$.

(A review on this topic is given in [11], but no globally stable scheme is yet given.)

B. Another Adaptive Observer Implementation

According to [25], since (8) is in Brunovsky observer form, the adaptive observer based on the filtered transformation ($z = x - M\theta$ with $M \in \mathbb{R}^{4\times 2}$) is devised as follows:

$$\begin{cases} p\hat{z} = A\hat{z} + \phi_0 + B\beta^T\hat{\theta} + KC(z - \hat{z}) \\ p\hat{\theta} = \Gamma\beta C\,(z - \hat{z}) \\ pM = (I_{4\times 4} - BC)\,(AM + \Phi) \\ \hat{x} = \hat{z} + M\hat{\theta} \end{cases} \tag{10}$$

where $\beta^T = C\,(AM + \Phi)$ is the new regressor, $\Gamma \in \mathbb{R}^{2\times 2}$ is the diagonal adaptation gain matrix, $B = \begin{bmatrix} I & cI \end{bmatrix}^T$ and $K = (A + kI_{4\times 4})B$ with $k, c \in \mathbb{R}_{>0}$. The PE condition follows as:

$$aI \le \int_t^{t+T} \beta(t)\beta^T(t)dt \le bI \tag{11}$$

with positive constants a, b, T for all t.

VI. Conclusion

The authors have presented the globally stable speed-adaptive observer that has not been stressed enough in the literature. By rearranging the electrical dynamics of IMs, the observer-based speed estimation can be achieved without any approximation, whose stability holds in all working conditions excluding the zero-frequency excitation. The effectiveness of the design is verified by experimental results, where the slow-speed-reversal test is carried out successfully and zero-frequency crossing is found to be possible. Additionally, the influence of uncertainty of stator resistance or total leakage inductance is analyzed through experimental results. At last, joint estimation of rotor resistance and rotor speed is discussed.

Appendix

The IM data acquired by the commercial inverter product (Mitsubishi FR-A700) are: $r_s = 3.04\ \Omega$, $r_{\text{req}} = 1.60\ \Omega$, $L_\sigma = 0.0249$ H, and $L_\mu = 0.448$ H.

The observer coefficients are: $\gamma_\omega = 1.2\text{e}7\ \text{Wb}^{-2}\text{s}^{-2}$, $\lambda_1 = 1\text{e}3\ \text{s}^{-1}$, and $\lambda_2 = 1.6\text{e}4\ \text{s}^{-2}$.

References

[1] L. Harnefors and M. Hinkkanen, "Stabilization methods for sensorless induction motor drives—A survey," *IEEE J. Emer. Sel. Topics Power Electron.*, vol. 2, no. 2, pp. 132–142, Jun. 2014.
[2] L. Harnefors, "Globally stable speed-adaptive observers for sensorless induction motor drives," *IEEE Transa. Ind. Electron.*, vol. 54, no. 2, pp. 1243–1245, Apr. 2007.
[3] J. Chen and J. Huang, "Online decoupled stator and rotor resistances adaptation for speed sensorless induction motor drives by a time-division approach," *IEEE Trans. Power Electron.*, vol. 32, no. 6, pp. 4587–4599, Jun. 2017.
[4] S. Suwankawin and S. Sangwongwanich, "A speed-sensorless IM drive with decoupling control and stability analysis of speed estimation," *IEEE Trans. Ind. Electron.*, vol. 49, no. 2, pp. 444–455, Apr. 2002.
[5] S. Suwankawin and S. Sangwongwanich, "Design strategy of an adaptive full-order observer for speed-sensorless induction-motor drives-tracking performance and stabilization," *IEEE Trans. Ind. Electron.*, vol. 53, no. 1, pp. 96–119, Feb. 2006.
[6] E. Etien, C. Chaigne, and N. Bensiali, "On the stability of full adaptive observer for induction motor in regenerating mode," *IEEE Trans. Ind. Electron.*, vol. 57, no. 5, pp. 1599–1608, May 2010.
[7] M. S. Zaky, M. k. Metwally, H. Azazi, and S. Deraz, "A new adaptive SMO for speed estimation of sensorless induction motor drives at zero and very low frequencies," *IEEE Trans. Ind. Electron.*, vol. 65, no. 9, pp. 6901–6911, Sep. 2018.
[8] L. Harnefors and M. Hinkkanen, "Complete stability of reduced-order and full-order observers for sensorless IM drives," *IEEE Trans. Ind. Electron.*, vol. 55, no. 3, pp. 1319–1329, Mar. 2008.
[9] H. Kubota, I. Sato, Y. Tamura, K. Matsuse, H. Ohta, and Y. Hori, "Regenerating-mode low-speed operation of sensorless induction motor drive with adaptive observer," *IEEE Trans. Ind. Appl.*, vol. 38, no. 4, pp. 1081–1086, Jul. 2002.
[10] M. Hinkkanen and J. Luomi, "Stabilization of regenerating-mode operation in sensorless induction motor drives by full-order flux observer design," *IEEE Trans. Ind. Electron.*, vol. 51, no. 6, pp. 1318–1328, Dec. 2004.
[11] J. Chen and J. Huang, "Stable simultaneous stator and rotor resistances identification for speed sensorless induction motor drives: Review and new results," *IEEE Trans. Power Electron.*, to be published.
[12] E. Dehghan-Azad, S. Gadoue, D. Atkinson, H. Slater, P. Barrass, and F. Blaabjerg, "Sensorless control of IM for limp-home mode EV applications," *IEEE Trans. Power Electron.*, vol. 32, no. 9, pp. 7140–7150, Sep. 2017.
[13] E. Dehghan-Azad, S. Gadoue, D. Atkinson, H. Slater, P. Barrass, and F. Blaabjerg, "Sensorless control of IM based on stator-voltage MRAS for limp-home EV applications," *IEEE Trans. Power Electron.*, vol. 33, no. 3, pp. 1911–1921, Mar. 2018.
[14] G. R. Slemon, "Modelling of induction machines for electric drives," *IEEE Trans. Ind. Appl.*, vol. 25, no. 6, pp. 1126–1131, Nov. 1989.
[15] K. S. Narendra and A. M. Annaswamy, *Stable Adaptive Systems*. Chelmsford, MA, USA: Courier Corporation, 1989.
[16] Y. Zheng and K. A. Loparo, "Adaptive flux and speed estimation for induction motors," in *Proc. 1999 Amer. Control Conf.*, 1999, vol. 4, pp. 2521–2525.
[17] Q. Zhang, "Adaptive observer for multiple-input-multiple-output (MIMO) linear time-varying systems," *IEEE Trans. Automat. Control*, vol. 47, no. 3, pp. 525–529, Mar. 2002.
[18] P. Vas, *Sensorless Vector and Direct Torque Control*. New York, NY, USA: Oxford Univ. Press, 1998.
[19] H. Kubota, "Closure to discussion of "regenerating-mode low-speed operation of sensorless induction motor drive with adaptive observer"," *IEEE Trans. Ind. Appl.*, vol. 39, no. 1, pp. 20–20, Jan. 2003.

[20] M. Montanari, S. M. Peresada, C. Rossi, and A. Tilli, "Speed sensorless control of induction motors based on a reduced-order adaptive observer," *IEEE Trans. Control Syst. Technol.*, vol. 15, no. 6, pp. 1049–1064, Nov. 2007.

[21] G. Wang, H. F. Hofmann, and A. El-Antably, "Speed-sensorless torque control of induction machine based on carrier signal injection and smooth-air-gap induction machine model," *IEEE Trans. Energy Convers.*, vol. 21, no. 3, pp. 699–707, Sep. 2006.

[22] J.-I. Ha and S.-K. Sul, "Sensorless field-orientation control of an induction machine by high-frequency signal injection," *IEEE Trans. Ind. Appl.*, vol. 35, no. 1, pp. 45–51, Jan. 1999.

[23] H. Toliyat, E. Levi, and M. Raina, "A review of RFO induction motor parameter estimation techniques," *IEEE Trans. Energy Convers.*, vol. 18, no. 2, pp. 271–283, Jun. 2003.

[24] H. Tajima and Y. Hori, "Speed sensorless field-orientation control of the induction machine," *IEEE Trans. Ind. Appl.*, vol. 29, no. 1, pp. 175–180, Jan./Feb. 1993.

[25] R. Marino and P. Tomei, "Global adaptive observers for nonlinear systems via filtered transformations," *IEEE Trans. Automat. Control*, vol. 37, no. 8, pp. 1239–1245, Aug. 1992.